crystals

MDPI

Article

Elucidation of the Conformational Transition of Oligopeptidase B by an Integrative Approach Based on the Combination of X-ray, SAXS, and Essential Dynamics Sampling Simulation

Vladimir V. Britikov [1,†], Vladimir I. Timofeev [2,3,*,†], Dmitry E. Petrenko [4,†], Elena V. Britikova [1], Alena Y. Nikolaeva [4], Anna V. Vlaskina [4], Konstantin M. Boyko [5], Anna G. Mikhailova [2] and Tatiana V. Rakitina [2,*]

1 Institute of Bioorganic Chemistry, National Academy of Sciences of Belarus, 220141 Minsk, Belarus; britikov@iboch.by (V.V.B.); britikova@iboch.by (E.V.B.)
2 Shemyakin-Ovchinnikov Institute of Bioorganic Chemistry of the Russian Academy of Sciences, 117997 Moscow, Russia; anna.mikhailova@ibch.ru
3 Federal Scientific Research Center "Crystallography and Photonics" of the Russian Academy of Sciences, 119333 Moscow, Russia
4 Complex of NBICS Technologies, National Research Center "Kurchatov Institute", 123182 Moscow, Russia; petrenko_de@nrcki.ru (D.E.P.); nikolaeva_ay@nrcki.ru (A.Y.N.); vlaskina_av@rrcki.ru (A.V.V.)
5 Bach Institute of Biochemistry, Research Centre of Biotechnology of the Russian Academy of Sciences, 119071 Moscow, Russia; kmb@inbi.ras.ru
* Correspondence: timofeev@ibch.ru (V.I.T.); rakitina@ibch.ru (T.V.R.)
† These authors contributed equally to this work.

Citation: Britikov, V.V.; Timofeev, V.I.; Petrenko, D.E.; Britikova, E.V.; Nikolaeva, A.Y.; Vlaskina, A.V.; Boyko, K.M.; Mikhailova, A.G.; Rakitina, T.V. Elucidation of the Conformational Transition of Oligopeptidase B by an Integrative Approach Based on the Combination of X-ray, SAXS, and Essential Dynamics Sampling Simulation. *Crystals* **2022**, *12*, 712. https://doi.org/10.3390/cryst12050712

Academic Editor: Borislav Angelov

Received: 20 April 2022
Accepted: 13 May 2022
Published: 17 May 2022

Abstract: Oligopeptidase B (OPB) is the least studied group from the prolyl oligopeptidase family. OPBs are found in bacteria and parasitic protozoa and represent pathogenesis factors of the corresponding infections. OPBs consist of two domains connected by a hinge region and have the characteristics of conformational dynamics, which include two types of movements: the bridging/separation of α/β-hydrolase catalytic and β-propeller-regulatory domains and the movement of a loop carrying catalytic histidine, which regulates an assembly/disassembly of the catalytic triad. In this work, an elucidation of the interdomain dynamics of OPB from *Serratia proteamaculans* (SpOPB) with and without modification of the hinge region was performed using a combination of X-ray diffraction analysis and small-angle X-ray scattering, which was complemented with an essential dynamics sampling (EDS) simulation. The first crystal structure of catalytically deficient SpOPB (SpOPBS532A) with an intact hinge sequence is reported. Similarly to SpOPB with modified hinges, SpOPBS532A was crystallized in the presence of spermine and adopted an intermediate conformation in the crystal lattice. Despite the similarity of the crystal structures, a difference in the catalytic triad residue arrangement was detected, which explained the inhibitory effect of the hinge modification. The SpOPBS532A structure reconstituted to the wild-type form was used as a starting point to the classical MD followed by EDS simulation, which allowed us to simulate the domain separation and the transition of the enzyme from the intermediate to open conformation. The obtained open state model was in good agreement with the experimental SAXS data.

Keywords: crystal structure; prolyl oligopeptidase; oligopeptidase B; intermediate state; hinge region; X-ray diffraction analysis; small-angle X-ray scattering; molecular dynamics; essential dynamics sampling

1. Introduction

Oligopeptidases B (OPBs, EC 3.4.21.83) are trypsin-like serine peptidases found in ancient parasitic protozoa and bacteria, and pathogenesis factors of parasitic and bacterial infections [1,2]. In the acute phases of the disease, these enzymes enter the blood of patients and hydrolyze several physiologically important peptides (including atrial natriuretic

factor), causing serious disorders in the hematopoiesis system [3]. In addition, OPBs provide a bacterial resistance toward proline-rich antimicrobial peptides [4].

OPBs represent the least studied group of prolyl oligopeptidases (POPs, family S9, clan SC), which include serine peptidases with dissimilar substrate specificity but similar spatial folding [5]. The representatives of the S9 family are distributed into subfamilies S9A–S9C [6]. OPBs, together with prolyl endopetidases (PEPs), form the S9A subfamily.

POPs consist of two domains: a C-terminal α/β-hydrolase catalytic domain and an N-terminal β-propeller domain (Figure 1A) [7]. Topologically, about 70 amino acids from the N-terminus belong to the catalytic domain. Two domains are connected by two hinge peptides: the first hinge connects the N-terminal region to the β-propeller; the second hinge is the β-propeller to the main part of the catalytic domain. The catalytic domain contains a catalytic triad composed of S, D, and H residues. The catalytic histidine is located on a very flexible loop (H-loop), the movement of which regulates the assembly and disassembly of the catalytic triad in the center of the interdomain cavity. The propeller domain performs a regulatory function, blocking access to the active center to bulk substrates larger than 30 amino acids. Such an architecture allows the enzymes to adopt different conformations, which were discovered by X-ray diffraction (XRD) studies [8–16] (Figure 1B).

Three conformations of POPs include a closed (catalytically active) state, in which the domains and residues of the catalytic triad are brought together [8–13], an open (inactive), in which the domains and residues of the catalytic triad are spatially separated [8–12], and an intermediate state, which combines the closeness of the domains with the disassembly of the catalytic triad [14–16]. In the absence of ligands, the bacterial PEPs and protozoan OPBs were captured in the open conformations [8,9,12], while the binding of inhibitors caused a transition to the closed states [8,9,12,13]. The intermediate states were observed in two cases: when archaeal PEP from *Pyrococcus furiosus* was crystallized with a substrate-like prolylproline ligand in the interdomain cavity [14] and when OPB from bacteria *Serratia proteamaculans* with a modified hinge (SpOPBmod) was crystallized in the presence of polyamine spermine [15,16]. It can be assumed that the intermediate state is the natural functional state of OPBs and PEPs in vivo, where the intracellular medium is enriched with various physiologically active molecules including polyamines and substrate-like molecules, respectively. Two-stage catalytic activation, in which the closure of domains precedes the convergence of the residues of the catalytic triad, may represent a gating mechanism for substrate selection [15]. As has been shown in numerous computational studies performed on the models of mammalian PEPs, which were crystallized only in the closed states, a central pore of the β-propeller, its open-Velcro topology (separation between the first and last blades), and opening in the interdomain interface provide numerous routes for the entrance of substrates and the exit of products [17–22].

It should be noted that according to the small-angle X-ray scattering (SAXS), not only spermine, but also the modification of the hinge itself affects the conformation of SpOPB in solution [15]. The modification also caused a significant inhibition of the SpOPBmod catalytic activity. Given the known pharmacological importance of OPBs [1–4,23,24], it can be assumed that the hinge region may serve as a prospective target for peptidometics or peptide-like inhibitors and its impact on the conformational transition of SpOPB should be carefully studied.

In this study, to further elucidate the conformational dynamics of SpOPB, we used an integrative approach, in which experimental X-ray-based methods (XRD analysis and SAXS) were complemented with essential dynamics sampling (EDS) simulations. Two experimental approaches provided information on the SpOPB conformations in the crystalline and liquid states, while a combination of classical molecular dynamics (MD) with EDS was used to model the conformational transition from the intermediate state observed in crystals to the open state observed in solution. EDS simulations are an advanced sampling method, which utilize the data of correlated motions from the results of the covariance analysis to guide the MD simulations. When a definition of the collective fluctuations with the largest amplitude is obtained from an initial MD simulation, EDS is used to manipulate

the position of a protein along the eigenvectors stimulating the system to explore new regions. Both types of SpOPB with and without the hinge region modification were involved in the research.

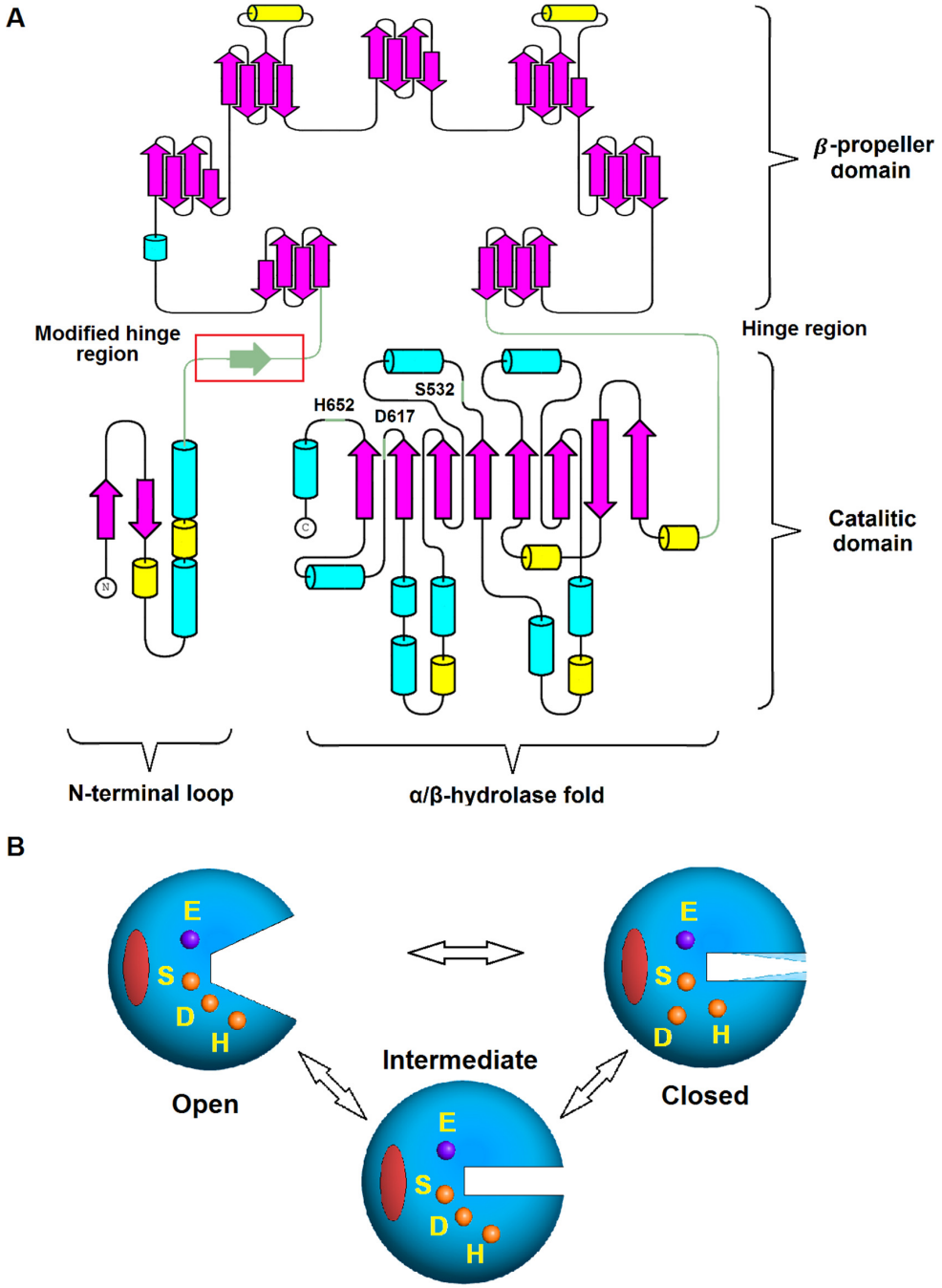

Figure 1. The structure and conformational states of POPs. (**A**) The schematic representation of a typical structure of POP demonstrates a domain swap in the catalytic domain. The topology was prepared using the SpOPB crystal structure. Secondary structure elements are shown in black (loops), cyan (α-helices), yellow (3_{10} helices), and magenta (β-strands). The residues of the catalytic triad are numbered according to the SpOPB sequence. Pale green shows the hinge peptides. The residues of the first hinge peptide IPQQEH, which were changed to ENLYFQ in SpOPBmod, are marked with a red square. (**B**) The schematic representation of the three conformations observed in the POP crystal structures. The residues of the catalytic triad and S1 substrate binding center are shown by the orange and violet balls, respectively; the hinge is a red ellipse.

As a result of XRD analysis, the first crystal structure of the catalytically deficient SpOPB (SpOPBS532A) with the intact hinge sequence was obtained as well as the new structures of the modified enzyme. Similarly to SpOPBs with modified hinges, SpOPBS532A was crystallized in the intermediate conformation. Despite the overall similarity of the crystal structures, an important difference was found in the arrangement of the catalytic D532, which could be the reason for the activity loss of the modified enzyme. The EDS simulation based on the results of the classical MD of the wild-type SpOPB allowed us to obtain the SpOPB open-state model, which was in good agreement with the experimental SAXS data. Thus, using an integrative approach, we were able to simultaneously solve two tasks: to understand why a change in the hinge region affects the catalytic activity of SpOPB, and to demonstrate that the EDS simulation can be successfully used in combination with the experimental SAXS profile to model protein conformations in solution.

2. Materials and Methods

2.1. Production of Recombinant Proteins

Preparation of SpOPB-, SpOPBS532A-, SpOPBmod-, and SpOPBmodS532A-expressing plasmids have been described in [15,25]. The expression of recombinant proteins was carried in the BL21(DE3)RIPL *Escherichia coli* strain (Novagen, Madison, WI, USA). All proteins were isolated and purified to homogeneity as described in [26]. Buffer exchange and protein concentration adjustment were performed with 30 kDa cutoff centrifugal filter devices (Millipore, Burlington, MA, USA). The quantity and quality of the protein samples were determined by the Bradford method and SDS-PAAG electrophoresis, respectively. Molar concentrations were calculated using titration with the p'-guanidinobenzoic acid p-nitrophenyl ester [27].

2.2. Crystallography, X-ray, and Structural Analysis

Protein samples for crystallization were prepared in 20 mM Tris–HCl, pH 8.0, and 100 mM NaCl buffer supplemented with 5 mM spermine. Protein concentrations were over 20.0 mg/mL. The starting crystallization condition was described in [28], and crystallization screening in [29]. Briefly, the crystallization was conducted at 4 °C, the final growth conditions were 0.2 M $C_3H_2O_4Na_2$, pH 7.0, 20–24% PEG 3350 (SpOPBmod); 0.2 M Li_2SO_4, 0.1 M Bis-Tris, pH 5.5, 27% PEG 3350 (SpOPBS532A). Paraton and glycerol were used for cryoprotection in the case of SpOPBmod and SpOPBS532A, respectively.

Diffraction data were collected at the SPring-8 synchrotron facility (Harima Science Garden City, Japan). The structures were solved by the molecular replacement method using the BALBES program [30]. Refinement and visual inspection of the electron density maps or manual rebuilding of the models were performed with the REFMAC5 program of the CCP4 suite [31] and the COOT interactive graphics program [32], respectively. Data collection and refinement statistics are presented in Table 1.

In all structures, an asymmetric unit contained one independent copy of the protein. Programs COOT [32], PyMOL Version 1.9.0.0 (Schrödinger, New York, NY, USA) and PDBePISA [33] were used for the visual inspection and comparison of the structures and analysis of the interdomain interfaces, respectively. The topology was prepared with TOPDRAW [34].

Table 1. Data collection, processing, and refinement.

PDB ID Proteins	**7ZJZ (SpOPBS532A)**	**7YWS (SpOPBmod)**	**7YX7 (SpOPBmod)**
Data collection			
Diffraction source	Spring 8	Spring 8	Spring 8
Wavelength (Å)	0.8	1	0.8
Temperature (K)	100	100	100
Detector	DECTRIS EIGER X 16 M	DECTRIS EIGER X 16 M	DECTRIS EIGER X 16 M
Space group	$P2_12_12_1$	$P2_12_12_1$	$P2_12_12_1$
a, b, c (Å)	72.86; 100.45; 108.92	72.40, 100.45, 108.66	72.95, 100.53, 108.88
α, β, γ (°)	90.0	90.0	90.0
Unique reflections	63693 (9183)	86543 (12364)	78,927 (12166)
Resolution range (Å)	30.0–1.90 (2.00–1.90)	30.0–1.70 (1.79–1.70)	30.0–1.72 (1.81–1.72)
Completeness (%)	99.96 (100.00)	98.80 (98.00)	92.50 (98.80)
Average redundancy	7.15 (2.27)	6.40 (6.16)	4.29 (4.67)
$\langle I/\sigma(I)\rangle$	3.32 (2.02)	9.46 (2.18)	3.33 (2.10)
* Rmrgd-F (%)	11.5 (57)	5.3 (35)	17.3 (32)
Refinement			
R_{fact} *(%)*	19.7	18.7	20.1
$R_{\text{free.}}$*(%)*	24.9	21.8	23.9
Bonds (Å)	0.009	0.011	0.011
Angles (°)	1.578	1.704	1.634
Ramachandran plot			
Most favored (%)	99.2	99.2	99.2
Allowed (%)	0.8	0.8	0.8
No. atoms			
Protein	5547	5545	5545
Water	398	518	607
Ligands	56	42	14
B-factor (Å^2)	40.059	25.270	15.470

Values in parenthesis are for the highest-resolution shell. * $\text{Rmrgd} - \text{F} = 2\sum_{hkl} |\langle I_1(hkl)\rangle - \langle I_2(hkl)\rangle| / \sum_{hkl} \langle I_1(hkl)\rangle - \langle I_2(hkl)\rangle$.

2.3. Data Bank Accession Numbers

The structures were deposited with the Protein Data Bank (PDB) under accession code (ID) 7ZJZ (SpOPBS532A), 7YWS (SpOPBmod), and 7YX7 (SpOPBmod).

2.4. SAXS Measurement and Data Analysis

SAXS experiments were carried out at the BM29 beamline at the ESRF (Grenoble, France) using a PILATUS3 2M photon counting detector (DECTRIS, Baden, Switzerland). Protein samples were prepared at three different protein concentrations (5, 2.5, and 1.25 mg/mL) in 20 mM Tris–HCl buffer, pH 8.0, and 100 mM NaCl and were measured at 20 °C. The sample delivery and measurements were performed using a 1 mm diameter quartz capillary, which is part of the BioSAXS automated sample changer unit. Before and after each sample measurement, the corresponding buffer was measured and averaged. All experiments were conducted with the following parameters: beam current—200 mA; flux—2.6 × 1012 photons/s; wavelength—1 A; estimated beam size—1 mm × 100 um. A total of 10 frames (one frame per second) were taken from each sample.

The BioXTAS RAW software package [35] was used for the processing of experimental SAXS profiles. All experimental SAXS profiles were analyzed in the Guinier region to check the possible intermolecular interaction or aggregation due to radiation damage. Theoretical scattering curves were calculated and compared with the experimental profile using FOXS [36].

2.5. Classical MD Simulation and Analysis

All MD simulations were performed using the GROMACS software package (2021.4 release) [37], compiled with CUDA support for GPU utilization (RTX 3090 GPU was used) and the Amber ff99SB-ILDN force field [38]. The crystal structure of SpOPBS532A was taken as the starting structure for the simulation with the substitution of alanine 532 to the serine residue (as in wild type). This substitution was made using the UCSF Chimera program tools [39]. The protein was solvated with water of the SPC type in a periodic rectangular box with a 1.2 nm distance between the solute and the box. The charge of the system was neutralized by substituting the solvent molecule with Na^+ and Cl^- ions up to the concentration of 0.15 M. The total number of atoms in the system was 117,541. For the system, equilibration was used as the standard protocol of simulation, which consists of a stage of minimization, NVT (for 100 ps), and NPT (for 100 ps) equilibration for the temperature and pressure stabilization. The temperature and pressure of the system were independently maintained using a modified Berendsen thermostat (V-rescale) and Parrinello–Rahman barostat algorithm at a constant temperature and pressure of 300 K and 1 bar, respectively. For the calculation of the long-range electrostatic interactions, we employed the particle mesh Ewald (PME) algorithm [40]. Finally, the production of the MD simulations were performed for 200 ns and the data were collected every 20 ps. The stability of the protein structure during the MD trajectory was checked by calculating the root mean square deviations (RMSD) for the backbone atoms and also by the prediction of the secondary structure content using the dssp algorithm [41,42]. All parameters for the MD trajectory analysis (RMSD, RMSF, Rg, SASA, etc.) were calculated using GROMACS subprograms (routines). The covariance analysis was utilized to obtain the eigenvectors and corresponding eigenvalues for further essential dynamics (ED) sampling simulation. Before the covariance matrix calculation and diagonalization, the protein structures from the trajectories were aligned by least square fitting to a reference structure.

2.6. Essential Dynamics Sampling (EDS) and Analysis

The EDS method was originally developed to overcome the sampling issue [43]. In this work, the EDS simulation was used to enhance the conformational sampling of the OpB structure to a rich open-state conformation. First, through the covariance analysis of the classical MD were calculated the eigenvectors and corresponding eigenvalues (using GROMACS gmx covar command), which are described as correlated essential protein motions. For these purposes, all protein structures from trajectories were fitted by least square fitting to a reference structure to remove the overall rotation and translation motion. Then, the covariance matrix (mass-weighted) was calculated and diagonalized to produce the eigenvectors with corresponding eigenvalues. The obtained data were further used to generate an essential dynamics sampling input file sam.edi with the gmx make_edi command using the first six eigenvectors for the determination of the EDS subspace. To perform the EDS simulation, the algorithm of the acceptance radius expansion along the selected eigenvectors was used by setting the maximum number of the sampling cycle parameter to 2000 and the slope parameter to 0.0004 nm/step (sets a minimum on the rate of expansion).

3. Results and Discussion

3.1. The Structures of SpOPB with an Intact and Modified Hinge Have Similar Fold but Different Arrangement of the Catalytic D617 Residue

The first crystal structure of the catalytically impaired SpOPBS532A (PDB ID 7ZJZ) with an intact hinge region was determined at a 1.9 Å resolution and compared with two novel structures of the enzyme with modified hinges (SpOPBmod), which were determined at the resolutions of 1.7 (PDB ID 7YWS) and 1.72 Å (PDB ID 7YX7), respectively (Table 1). The modification affected the first hinge peptide (residues 71–76), whose sequence IPQQEH was changed to ENLYFQ (Figure 1A). This mutation introduced the cleavage site of the tobacco etch virus protease into the first hinge peptide [15]. The modified enzyme had similar physicochemical characteristics but significantly reduced catalytic activity compared to the wild-type enzyme [15]. The Cα-atom superposition of the SpOPBS532A structure on the SpOPBmod structures 7YWS and 7YX7 provided the same RMSD value of 0.4 Å. The superposition of the two SpOPBmod structures provided a RMSD of 0.3 Å. Similar RMSD values were obtained upon the superposition of the novel structures with the previously reported SpOPBmod structure (PDB ID 7OB1, [15]). Since the new structures had better resolutions than the previously reported one, they were used to study the contribution of the hinge modification to the protein folding and dynamics.

All structures showed a similar two domain-folding of the polypeptide chains consisting of the α/β-hydrolase domain and the 7-bladed β-propeller domain, which is a characteristic of the POP family (Figure 2A). The distribution of residual RMSD values derived from the superposition of the SpOPBS532A structure on the SpOPBmod structures (7YWS and 7YX7) and those of the residual B-factors for the compared structures along the polypeptide chain are shown in Figure 2B. The bursts on the residual RMSD graph repeat the bursts of B-factors, which indicates that the differences in structures with intact and modified hinges are mainly concentrated in the most flexible regions. According to the residual B-factor distribution, the most flexible area of the SpOPB polypeptide chain is the H-loop of the catalytic domain (residues 649–658), which due to its disordering usually has a very poor electron density in the crystal structures of PEPs in the open states (Figure 2A–C). The second flexible area is a loop of the β-propeller located opposite the H-loop (residues 192–196). This loop was referred to as the latching loop due to its involvement in the substrate gating [19–21]. Unlike PEPs, in OPBs, this loop is noticeably shortened [13], and because of this, it is not able to independently regulate access to the interdomain space through an opening in the interface between domains. Other loops adjacent to the H-loop and latching loop and forming the interface between the domains as well as those that surround the hole at the top of the β-propeller also had noticeable mobility. It should be noted that the first hinge was much more flexible than the second one (Figure 2A).

The spermine molecules, in whose presence the proteins have been crystallized, accumulated in the large cavity between the catalytic and β-propeller domains (Figure 2A). Two spermines occupied similar positions in the SpOPBS532A and SpOPBmod (7YWS) structures: one close to the inner surface of the catalytic domain and another at the entrance to the internal space of the β-propeller. There was a third spermine molecule in the SpOPBS532A structure, which was located near the top entrance to the internal space of the β-propeller. No spermines were found in the interdomain space of the SpOPBmod (7YX7) structure. In all structures, one spermine per polypeptide was found outside the interdomain cavity, where it participated in the crystal lattice formation (Figure 2C,D).

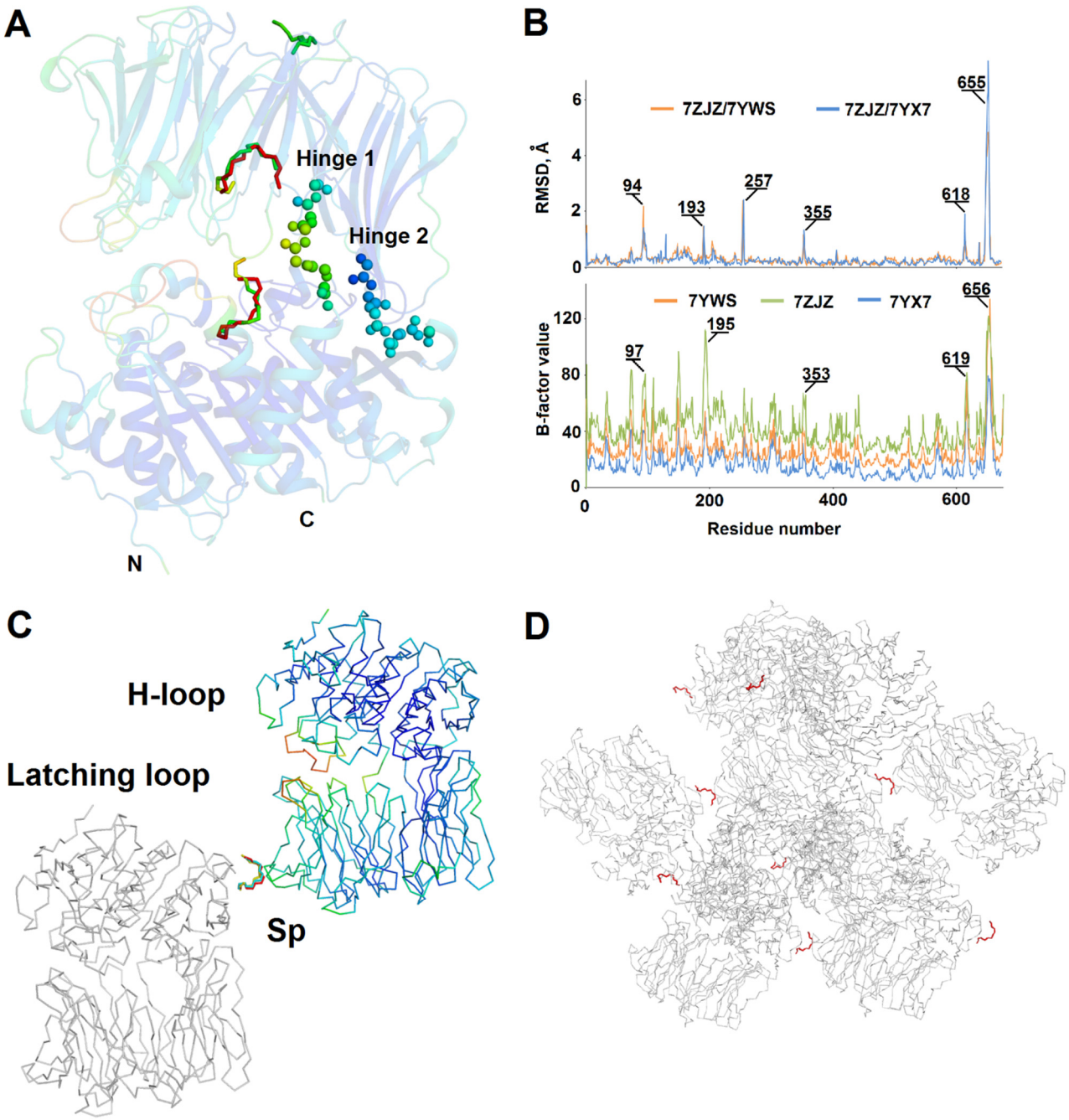

Figure 2. Comparative overview of the crystal structures obtained for enzymes with intact and modified hinge peptides. (**A**) The cartoon presentation of the SpOPBS532A structure (PDB ID 7ZJZ) colored according to the residual B-factors with spermines (shown in sticks) in the interdomain space. The aligned spermines from the SpOPBmod structure (PDB ID 7YWS) are colored in red. The main chain atoms of the hinge peptides are marked with balls. N- and C- denote N- and C-termini, respectively. (**B**) Residual RMSD values derived from C*a*-atom superpositions of the 7ZJZ structure over the 7YWS and 7YX7 structures and residual B-factor values obtained for all of the compared crystal structures. Residues, which have the highest RMSD and B-factors, are marked. (**C**) The conserved spermine molecule outside of the interdomain space connects the catalytic domain of one polypeptide with the β-propeller domain of another. Spermines (Sp) from 7ZJZ, 7YWS, and 7YX7 are colored by the B-factor value in red and orange, respectively. One polypeptide was colored according to the residual B-factors and the most flexible H-loop and latching loop are indicated. (**D**) Participation of spermines (red) in the crystal lattice formation.

In the crystal structures of protozoan OPBs, archaeal AAP, and bacterial PEPs, two conformations of the enzyme were observed [8–13]. In the closed (catalytically active) state, the domains and residues of the catalytic triad were brought together, while in the open (inactive) state, the domains and residues of the catalytic triad were spatially separated (Figure 1B). When the first structure of the bacterial OPB was obtained, in order to determine in which conformation the protein crystallized, the comparative analysis of the location of the domains and the arrangement of the catalytic triad residues was carried out [15]. This included measuring the distance between the centers of mass of the domains and the evaluation of the interface between them. In parallel, the distances between the residues of the catalytic triad were measured, primarily between the most stable serine and histidine, the movement of which actually determines the assembly and disassembly of the triad. The obtained parameters were compared with those derived from the crystal structures of PEPs in the open and closed states reported in [8,9,12]. It was found that SpOPBmod crystallized in the intermediate state, which combined the proximity of domains from the closed state and separation of the catalytic triad from the open state [15]. A similar analysis of the SpOPBS532A structure and the novel structures of the modified enzyme was performed (Table 2). Homologous models of the wild-type SpOPB in the open and closed conformations reported in [25] were included in the analyses as references. All of the analyzed parameters showed that the convergence of domains occurred without the assembly of the catalytic triad (i.e., both the SpOPBS532A and two SpOPBmods adopted intermediate conformations in the crystal lattices).

Table 2. Similar domain positioning and catalytic triad arrangements were observed in the SpOPB crystal structures obtained for enzymes with intact and modified hinge peptides.

Protein/Conformation	SpOPBS532A	SpOPBmod		Open	Closed
PDB ID	7ZJZ	7YWS	7YX7	Homologue Models	
The distance between the centers of mass of the domains, Å	32.3	32.0	32.2	37.1	30.3
Buried surface area [1], cat./prop. domain, %	11.7/9.8	11.9/10.1	11.6/9.9	6.9/6.8	14.8/12.5
Interface residues [2], cat./prop. domain, %	15.7/15.3	16.0/16.2	16.6/15.9	10.7/9.7	20.5/18.2
Catalytic Ser—His Cα-distance, Å	17.9	18.2	18.3	18.8	8.6
Catalytic Ser Oγ—His Nε2 distance, Å	NA *	13.1	13.1	16.7	2.8

[1]—% of the buried surface area over the total surface area of the domain according to the PDBePISA [33]. [2]—% of residues in the interface over the total residues in the domain according to the PDBePISA [33]. *—due to the S532A mutation.

The catalytic triad arrangements in the SpOPBS532A structure with the intact hinge and in the SpOPBmod structure (7YWS) with the modified hinge are shown in Figure 3. Both the catalytic S532 residue and A532 from SpOPBS532A are equally stabilized by numerous contacts of their main chains with the residues from their nearest surroundings whereas the D617 residues and the loops on which they are located (residues 616–621) have different degrees of mobility. As we already reported in [15], in the crystal structure of SpOPBmod (PDB ID 7OB1), the position of the catalytic D617 was stabilized due to the side chain-side chain interaction with R151 from the β-propeller. The same interactions were observed in the novel SpOPBmod structures (D617OD1/2-R151NH1/2 distances were 3–3.2 Å). Surprisingly, in the SpOPBS532A structure, the side chains of both R151 and D617 were not directed toward each other; instead, the side chain of D617 interacted with the main chain of the neighboring S618 (D617OD1–S618N distances was 3.05 Å) and as a result, the entire D617 loop became more flexible. Since in SpOPBS532A with the intact hinge, the R151–D617 interaction does not occur, it can be assumed that in SpOPBmod, this interaction, which fixes D617 in a position not favorable for the convergence of H652 and S532 and consequent catalytic activation, is associated with the hinge modification. This assumption is in full accordance with the previously established facts that the modification of the hinge significantly reduces the activity of the enzyme [15], while the amino acid

substitutions of R151 do not cause any inhibitory effect [26]. Unlike D617, the position and environment of catalytic H652 are approximately the same in the enzymes with intact and modified hinges. Both the histidine itself and the H-loop residues surrounding it are exceptionally mobile compared to other parts of the molecule. In addition to the residues of the H-loop, S149 from the β-propeller was observed in the immediate vicinity of H652.

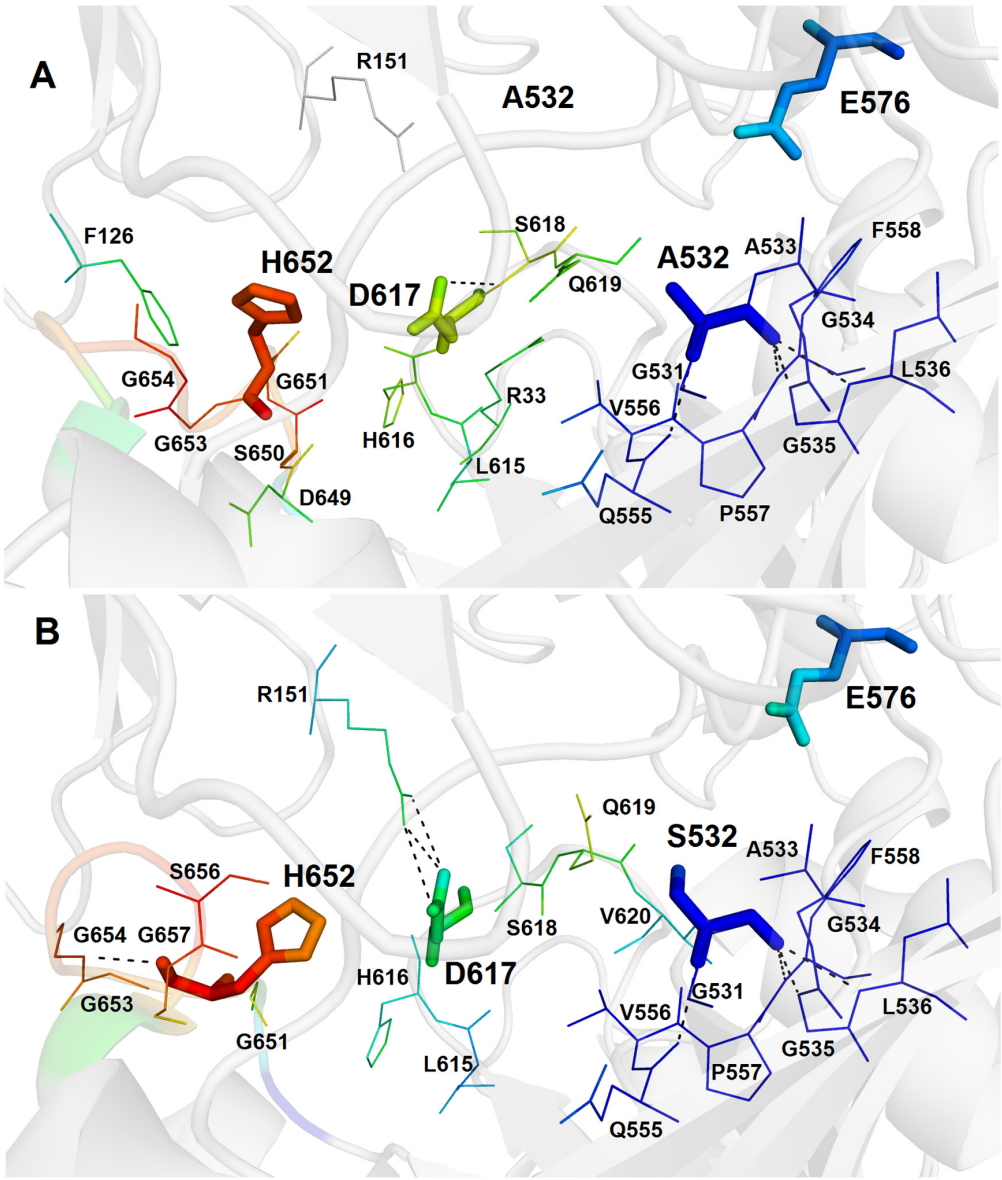

Figure 3. The catalytic triad arrangement in the 4 Å radius in the SpOPBS532A (**A**) and SpOPBmod (7YWS) (**B**) structures. All residues are shown with sticks and are colored according to their B-factor values. The E576 residues of the S1 substrate-binding center and the catalytic triad residues are enlarged. The polar contacts are shown by dotted lines.

The comparison of the original hinge peptide (IPQQEH) in the SpOPBS532A structure and the modified one (ENLYFQ) in the SpOPBmod structure (7YWS) is shown in Figure 4. The intact and modified variants had a similar composition of aliphatic, charged, and polar residues but a different order of the charge distribution. In both cases (independently from the modification), the main chains of the hinge peptides were stabilized by polar contacts with the adjacent areas of the catalytic and β-propeller domains, and with the second hinge peptide including the I/E71N-V68O, E/F75O-F91N, H/Q76O-K402NZ, I/E71O-K407NZ interactions, respectively. In addition, F75 from the modified hinge interacted with F91

through both the main chains (F75N-F91O) and phenyl rings of the side chains. The residues L73 and Y74 from the modified hinge were stabilized by hydrophobic interactions with P93 and Y662 from the N-terminal and the main parts of the catalytic domain, respectively. These additional interactions reduced the mobility of the modified hinge compared to the intact one. Moreover, this seemingly small decrease in the local mobility affected both the dynamics of the entire molecule and its catalytic activity. As we have described above, there was a difference in the arrangement of the catalytic D617, and, according to the SAXS data, even in the absence of spermine, when SpOPB and SpOPBS532A had open conformations (see below), both open and intermediate conformations were observed in the SpOPBmod solution. The increased lability of the wild-type protein was also indicated by the fact that the residual B-factor of the SpOPBS532A structure exceeded those of the SpOPBmod structures (Figure 2B). This is why the SpOPBS532A structure (with restored catalytic S532) was chosen as the starting point for the artificial transfer of the protein from the intermediate (crystal-associated) state to the open (solution-associated) state using EDS simulation.

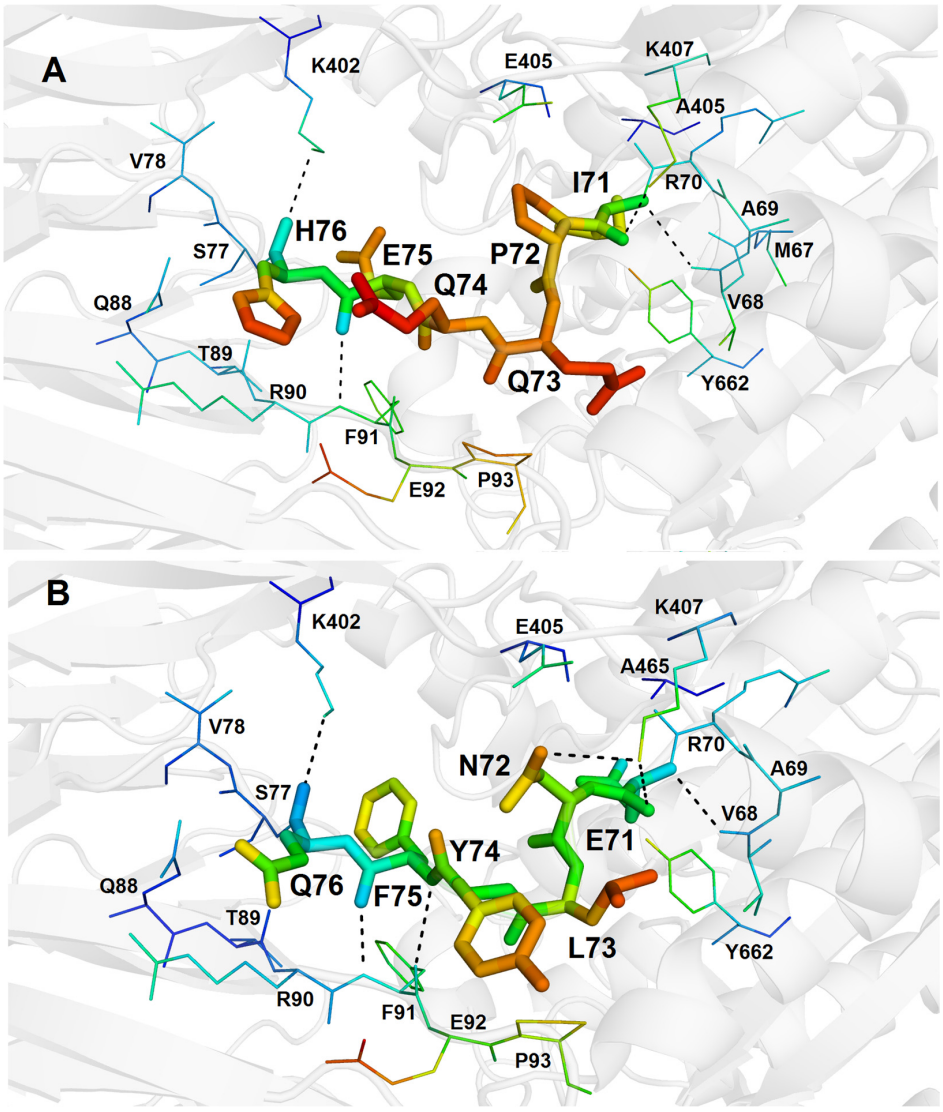

Figure 4. Comparison of the intact and modified hinge regions. (**A**) The amino acid surroundings in the 4 Å radius and polar contacts (dotted lines) of the intact hinge region in the SpOPBS532A structure (PDB ID 7ZJZ). (**B**) Similar representation of the modified hinge in the SpOPBmod structure (PDB ID 7YWS). All residues are shown in sticks and are colored according to the B-factor values. The residues from the first hinge peptide are enlarged.

3.2. Simulation of the Transition of SpOPB from the Intermediate to Open Conformation Using the Combination of Classical Molecular Dynamics and Essential Dynamics Sampling

As we have discussed above, three conformations of OPBs have been described: closed, intermediate, and open. Only the first conformation represents an active enzyme in which the catalytic triad is properly assembled. Thus, there are two possible ways for catalytic activation: one step transition from the open to closed state or two-step transition, when the domain closure precedes the assembly of the catalytic triad. Both pathways can occur in nature and the choice between them is most likely determined by the cellular environment. The understanding of the molecular mechanisms that drive the dynamic processes of the transitions may shed light on both the functioning of the enzyme and the possible approaches to its inhibition. According to the SAXS data, in solution, SpOPB has an open conformation [15], whose structure has been predicted by the homology modeling [26]. Spermine caused the transition to the intermediate state [15], similar to those observed in the crystal structures of SpOPBmod and SpOPBS532A described above. In this work, we decided to apply the computational approaches to simulate the reverse transition of the enzyme from the intermediate state to an open one. The SpOPBS532A structure with the recovered S532 was used for the modeling. The advanced sampling simulation method was chosen, since with the classical MD, it is difficult (or not possible) to achieve the desired transition.

The EDS allows one to sample the protein conformational space more efficiently than by classical MD. It has been successfully used in other studies of protein conformational transitions [44–46]. The peculiarity of the EDS technique is that the system moves along its essential eigenvectors as obtained from the analysis of the unbiased MD simulation, which provided a definition of the collective fluctuations, with the largest amplitude obtained by the covariance or normal mode analysis. At first, we performed the classical MD simulation and obtained the 200 ns productive trajectory, the analysis of which showed the preservation of the protein secondary structure (Supplementary Figure S1). The RMSD for the backbone atoms fluctuated within 0.1 nm, which indicates the stability of the intermediate conformation during the MD simulation (Figure 5A). Visual inspection of the trajectory allowed us to assert that, indeed, the transition to the open conformation did not appear. The gyration radius (R_g) of protein fluctuated within 2.67 nm and after 150 ns, and even decreased to 2.64 nm, which corresponded to a tighter closure of the two domains of SpOPB (Figure 5B). The theoretical SAXS curve for the average MD structure was well fitted to the experimental SAXS profile for SpOPB in the spermine-bound (intermediate) state (hi2–3.7) (Figure 5C), but did not fit to the experimental SAXS profile for spermine-free SpOPB in the open state (hi2–29.4) (Figure 5D). The same comparison of the theoretical SAXS curve for the SpOPBS532A crystal structure indicates that the latter is not consistent with the SAXS data for the spermine-free SpOPB and less consistent with the spermine-bound OpB structure than the average MD structure. Thus, one can conclude that during MD simulation, the SpOPB conformation approaches the real structure in solution compared to the crystal, but still remains within the intermediate conformation observed in the crystalline state.

Next, we analyzed the per-residue RMSF over the entire MD trajectory (Figure 5E) and compared it with the B-factors of the SpOPBS532A and SpOPBmod crystal structures (Figure 2B). We found that there was a strong correlation between the values of the B-factor and the RMSF from MD. The maximum similarity was observed in the loops containing residues R150, K194, D617, and H652. The last two residues were components of the catalytic triad; therefore, it can be assumed that the flexibility of the corresponding loops can contribute to the assembly/disassembly of the catalytic center.

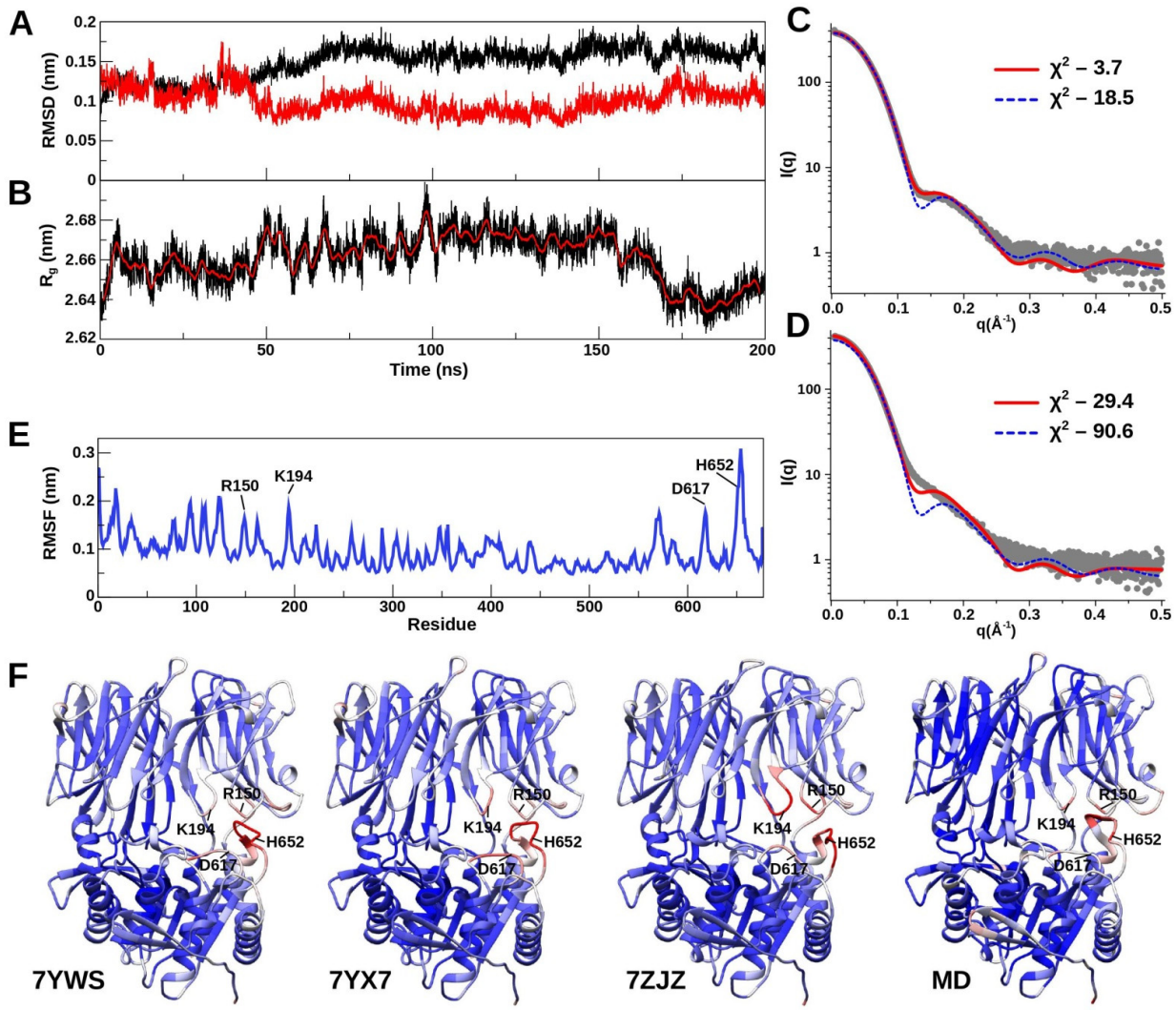

Figure 5. Comparison of the results of the 200 ns MD simulation of SpOPB with the SAXS data and the crystal structures of SpOPBmod and SpOPBS532A. The SpOPBS532A structure with the recovered S532 was used for modeling. (**A**) The standard deviation of the main chain atoms on the MD trajectory (the black line is the RMSD relative to the initial structure, and the red line is the RMSD relative to the average structure). (**B**) The change in the radius of gyration (R_g) (the red line is the average of 100 frames). (**C**) The experimental SAXS profile of SpOPB in the presence of spermine (gray dots) fitted to the theoretical curves for the averaged structures from the MD simulation (red solid line) and the SpOPBS532A crystal structure (blue dashed line). (**D**) A similar overlay of the theoretical curves on the experimental SAXS profile obtained for the free SpOPB (gray dots). (**E**) Per residue RMSF for the entire MD trajectory and the mobilities of the key residues are correlated with the enhanced B-factors from the crystal structures. (**F**) The crystal structures of SpOPBmod and SpOPBS532A, colored by the B-factors, and the averaged structure from the MD simulation, colored by RMSF. Red means the maximum values, blue means the minimum values.

In the next step, we applied the EDS simulation technique along the direction of the eigenvectors obtained by the covariance analysis to transfer SpOPB from the intermediate to open conformation. The starting structure was one from the classical MD. At first, we performed a covariance analysis of the classical MD trajectory and obtained the eigenvectors of the main correlated motions and their corresponding eigenvalues. For the EDS simulation, the first six eigenvectors (Supplementary Figure S2) were used, since they were responsible for the bulk of the movements of the polypeptide chain (Supplementary Figure S3). The simulation was performed using the algorithm of the acceptance radius

expansion along the selected eigenvectors. A 100 ns trajectory was produced. The EDS parameters and the length of the trajectory were selected in the preliminary simulations. The resulting trajectory consisted of 25,000 frames, which are required for more accurate analysis. Throughout the EDS trajectory, the secondary structure of the protein did not undergo significant changes (Supplementary Figure S4). Visual inspection of the trajectory showed that the SpOPB conformation changed gradually from the intermediate to open state. This was confirmed by analyzing the values of R_g, the solvent accessible surface area (SASA), and the backbone RMSD compared to the starting structure (Figure 6A–C). During the filtration stage, one section from the MD trajectory was selected for the comparison with the experimental SAXS profile. In the selected section (highlighted by the red stripe in Figure 6), R_g was in the range from 61 to 68 ns and reached 2.75 nm (Figure 2C).

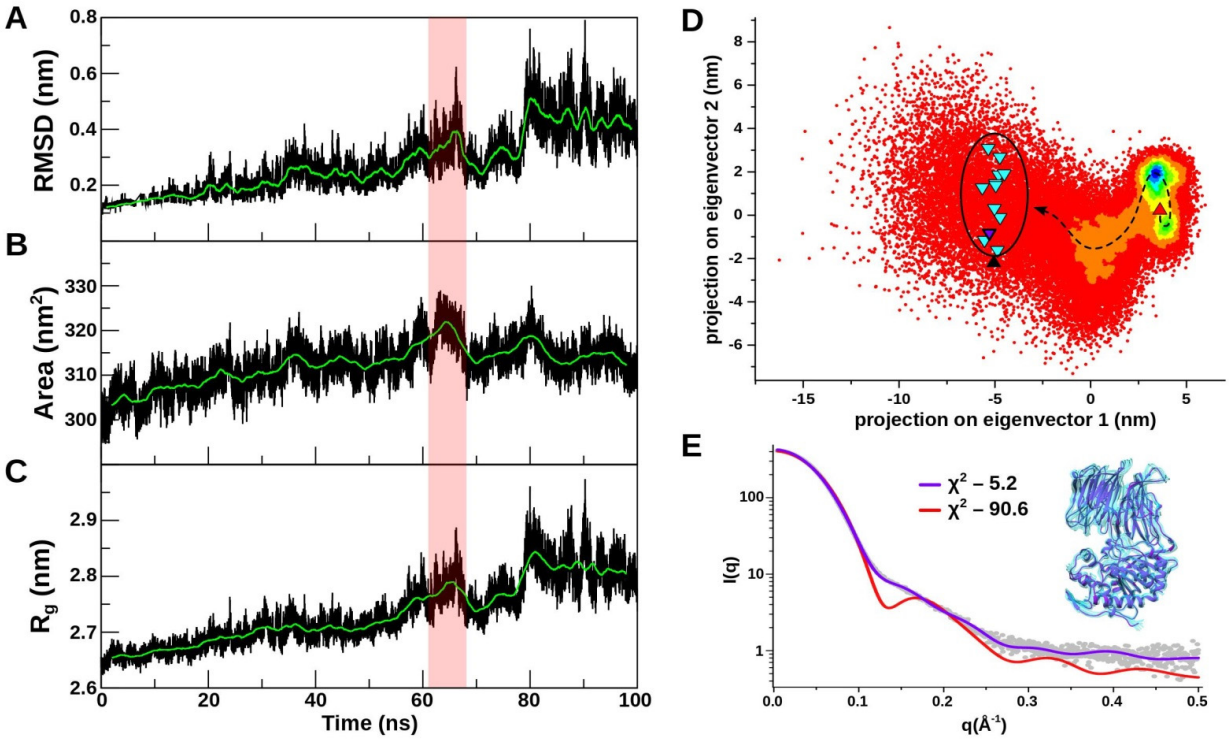

Figure 6. Comparison of the results of the ED/MD simulation of SpOPB with thee SAXS data and the SpOPBS532A crystal structure. The EDS trajectory (100 ns) obtained for SpOPB using six eigenvectors of the main motions (modes) from the correlation analysis (PCA) according to the classical MD. (**A**) The RMSD of the Ca atoms during the MD trajectory. (**B**) Change in the SASA for protein. (**C**) Change in the radius of gyration (R_g). The MD parameters corresponded to the classic MD with the exception of the settings for EDS. The total number of frames was 25,000. The trajectory section highlighted in red was used for the comparative analysis with the SAXS data obtained for the free SpOPB. This section had an Rg value in the range from 2.75 nm. (**D**) The projection of the combined EDS trajectory onto the two-dimensional space was defined by the first two eigenvectors. Each point in space denotes a separate structure. The density of points on the projection is determined by color (the transition from red to blue corresponds to an increase in density). The dashed line indicates the approximate direction of the trajectory (from the starting structure). Triangles denote the conformational positions of the selected structures. The colors of the triangles are as follows: red is the initial crystal structure of SpOPB in the intermediate state, black is a homologous model of the open conformation of the protein, triangles with the top down are the best structures from EDS, purple is for the best fit to the SAXS data. (**E**) Experimental SAXS profile for the spermine-free SpOPB (gray dots) with the superimposition of the theoretical curves for the best EDS structure (violet line) and the SpOPBS532A crystal structure (red line). The insert shows the aligned 12 best structures from the EDS (the structure with the best hi2 is purple, the rest are turquoise).

The structures from further parts of the trajectory were not analyzed due to the specifics of the EDS simulation with the radius expansion algorithm, since it can lead to the "over-reopened" conformational state. The selected trajectory range also correlated well with both the SASA (Figure 6B) and RMSD changes (Figure 6A) and stands out as a distinct transition (jump) region. A total of 1600 frames from this region were used for the analysis, in which 1600 theoretical SAXS curves from these frames were compared with the experimental SAXS profile for SpOPB in the free state. As a result, structures with a hi2 less than 6 were selected. This hi2 value corresponds to that obtained upon the comparison of the SAXS data with the homologous model of SpOPB in the open state [26].

There were 200 structures with chi2 in the range from 5.2 to 6. The 12 best structures according to chi2 values were analyzed relative to its position in the space of the 2D projection of the first two main eigenvectors, which was obtained by the covariance analysis of the combined trajectory composed of the classical MD and EDS (Figure 6D). These 12 structures fell within the narrow region of the first eigenvector, but spread within the second eigenvector. According to the results of the SAXS experiments, the structures from this region corresponded to the open conformation of SpOPB as well as to the homologous model of the SpOPB in the open conformation (Figure 6D,E). The spread of these structures in the conformational space can correspond to the real ensemble of closely related structures in open conformations in solution. The theoretical SAXS curve for the best EDS structure fit well with the experimental SAXS profile for the free state of SpOPB in contrast to the crystal structure of SpOPBS532A (Figure 6E).

4. Conclusions

Summarizing the results obtained using the EDS methodology, we can state that during the simulation, which began with an intermediate conformation, an open conformation of the protein was achieved, and this open conformation corresponded with a high degree of probability to the conformation observed in the SAXS experiment. This indicates that the approach used can be applied to simulate other transitions between the different conformational states found in structural studies of OPBs and PEPs [8–14].

In conclusion, we would like to emphasize the connection between the two main vectors of this research: the biological and methodological. Using the XRD and SAXS methods, we were able to determine the influence of the hinge region on the structural and dynamic properties of SpOPB in crystal and solution. This is what made it possible to choose the optimal initial structure and methodology of the computer modeling as well as to confirm that the open conformation obtained in silico corresponded to the one that actually exists in solution. Thus, we can conclude that the successful modeling of the conformational transition in silico is inextricably linked and complements the obtained biological data and emphasizes the biological significance of the work, at the same time, the result of EDS modeling indicates the possibility of applying the proposed approach to solving similar biological problems.

Supplementary Materials: The following supporting information can be downloaded at: https://www.mdpi.com/article/10.3390/cryst12050712/s1, Figure S1: Evolution of secondary structure of the SpOPB during the classical MD simulation calculated by DSSP algorithm.; Figure S2: Components of the first six eigenvectors from covariance analysis of the classical MD trajectory; Figure S3: Eigenvalues obtained from covariance analysis of MD trajectories; Figure S4: Evolution of secondary structure of the SpOPB during EDS simulation calculated by DSSP algorithm.

Author Contributions: Conceptualization, D.E.P., V.V.B. and T.V.R.; Methodology, E.V.B., V.V.B., V.I.T., A.V.V., K.M.B. and A.G.M.; Software, D.E.P., V.I.T., E.V.B. and V.V.B.; Validation, D.E.P., V.I.T., E.V.B. and V.V.B.; Investigation, D.E.P., A.Y.N., A.V.V., K.M.B., A.G.M. and T.V.R.; Resources, A.Y.N., A.G.M. and T.V.R.; Data Curation, D.E.P., V.I.T., E.V.B., V.V.B., K.M.B., A.G.M. and T.V.R.; Writing—Original Draft Preparation, D.E.P., V.V.B., A.G.M. and T.V.R.; Writing—Review & Editing, E.V.B., V.V.B. and T.V.R.; Visualization, E.V.B., D.E.P., V.V.B. and V.I.T.; Supervision, T.V.R.; Project Administration, T.V.R.; Funding Acquisition, T.V.R. All authors have read and agreed to the published version of the manuscript.

Funding: This research was funded by the Russian Science Foundation, grant number 21-74-20154 (structural study of SpOPB with the intact and modified hinge region).

Institutional Review Board Statement: Not applicable.

Informed Consent Statement: Not applicable.

Data Availability Statement: The article or supplementary materials contained the data. Structural data have been deposited at the RCSB data bank with accession codes—7ZJZ, 7YWS, and 7YX7.

Acknowledgments: We acknowledge the European Synchrotron Radiation Facility for the provision of synchrotron radiation facilities; Anton M. Popov for performing the SAXS experiment, and the structural biology group for their assistance in using the BM29 beamline. We acknowledge the Russian Federal Space Agency for providing an opportunity to participate in the crystallization in microgravity program (grant 8418.20.05) and the Ministry of Science and Higher Education of the Russian Federation (FSRC "Crystallography and Photonics" RAS) for their assistance in the X-ray experiment. We would like to thank the Center for the collective use of the "Bioorganika" of the Shemyakin–Ovchinnikov Institute of Bioorganic Chemistry RAS and Resource Center for Molecular and Cellular Biology of NRC "Kurchatov Institute" for their technical support.

Conflicts of Interest: The authors declare no conflict of interest. The funders had no role in the design of the study; in the collection, analyses, or interpretation of data; in the writing of the manuscript or in the decision to publish the results.

References

1. Motta, F.N.; Azevedo, C.D.S.; Neves, B.P.; de Araújo, C.N.; Grellier, P.; de Santana, J.M.; Bastos, I.M.D. Oligopeptidase B, a missing enzyme in mammals and a potential drug target for trypanosomatid diseases. *Biochimie* **2019**, *167*, 207–216. [CrossRef] [PubMed]
2. Coetzer, T.H.; Goldring, J.P.D.; Huson, L.E. Oligopeptidase B: A processing peptidase involved in pathogenesis. *Biochimie* **2008**, *90*, 336–344. [CrossRef] [PubMed]
3. Morty, R.E.; Pellé, R.; Vadász, I.; Uzcanga, G.L.; Seeger, W.; Bubis, J. Oligopeptidase B from Trypanosoma evansi. *J. Biol. Chem.* **2005**, *280*, 10925–10937. [CrossRef] [PubMed]
4. Mattiuzzo, M.; De Gobba, C.; Runti, G.; Mardirossian, M.; Bandiera, A.; Gennaro, R.; Scocchi, M. Proteolytic Activity of Escherichia coli Oligopeptidase B Against Proline-Rich Antimicrobial Peptides. *J. Microbiol. Biotechnol.* **2014**, *24*, 160–167. [CrossRef]
5. Polgár, L. The prolyl oligopeptidase family. *Cell. Mol. Life Sci. CMLS* **2002**, *59*, 349–362. [CrossRef]
6. Rawlings, N.D.; Barrett, A.J.; Thomas, P.D.; Huang, X.; Bateman, A.; Finn, R.D. The MEROPS database of proteolytic enzymes, their substrates and inhibitors in 2017 and a comparison with peptidases in the PANTHER database. *Nucleic Acids Res.* **2018**, *46*, D624–D632. [CrossRef]
7. Rea, D.; Fülöp, V. Structure-Function Properties of Prolyl Oligopeptidase Family Enzymes. *Cell Biophys.* **2006**, *44*, 349–365. [CrossRef]
8. Shan, L.; Mathews, I.I.; Khosla, C. Structural and mechanistic analysis of two prolyl endopeptidases: Role of interdomain dynamics in catalysis and specificity. *Proc. Natl. Acad. Sci. USA* **2005**, *102*, 3599–3604. [CrossRef]
9. Li, M.; Chen, C.; Davies, D.R.; Chiu, T.K. Induced-fit Mechanism for Prolyl Endopeptidase. *J. Biol. Chem.* **2010**, *285*, 21487–21495. [CrossRef]
10. Harmat, V.; Domokos, K.; Menyhárd, D.K.; Palló, A.; Szeltner, Z.; Szamosi, I.; Beke-Somfai, T.; Náray-Szabó, G.; Polgár, L. Structure and Catalysis of Acylaminoacyl Peptidase. *J. Biol. Chem.* **2011**, *286*, 1987–1998. [CrossRef]
11. Menyhárd, D.K.; Orgován, Z.; Szeltner, Z.; Szamosi, I.; Harmat, V. Catalytically distinct states captured in a crystal lattice: The substrate-bound and scavenger states of acylaminoacyl peptidase and their implications for functionality. *Acta Crystallogr. Sect. D Biol. Crystallogr.* **2015**, *71*, 461–472. [CrossRef]
12. Canning, P.; Rea, D.; Morty, R.E.; Fülöp, V. Crystal Structures of Trypanosoma brucei Oligopeptidase B Broaden the Paradigm of Catalytic Regulation in Prolyl Oligopeptidase Family Enzymes. *PLoS ONE* **2013**, *8*, e79349. [CrossRef] [PubMed]
13. McLuskey, K.; Paterson, N.; Bland, N.D.; Isaacs, N.W.; Mottram, J. Crystal Structure of Leishmania major Oligopeptidase B Gives Insight into the Enzymatic Properties of a Trypanosomatid Virulence Factor. *J. Biol. Chem.* **2010**, *285*, 39249–39259. [CrossRef] [PubMed]
14. Ellis-Guardiola, K.; Rui, H.; Beckner, R.L.; Srivastava, P.; Sukumar, N.; Roux, B.; Lewis, J.C. Crystal Structure and Conformational Dynamics of Pyrococcus furiosus Prolyl Oligopeptidase. *Biochemistry* **2019**, *58*, 1616–1626. [CrossRef] [PubMed]
15. Petrenko, D.E.; Timofeev, V.I.; Britikov, V.V.; Britikova, E.V.; Kleymenov, S.Y.; Vlaskina, A.V.; Kuranova, I.P.; Mikhailova, A.G.; Rakitina, T.V. First Crystal Structure of Bacterial Oligopeptidase B in an Intermediate State: The Roles of the Hinge Region Modification and Spermine. *Biology* **2021**, *10*, 1021. [CrossRef]
16. Timofeev, V.I.; Petrenko, D.E.; Agapova, Y.K.; Vlaskina, A.V.; Karlinsky, D.M.; Mikhailova, A.G.; Kuranova, I.P.; Rakitina, T.V. The Crystal Structure of Nα-p-tosyl-lysyl Chloromethylketone-Bound Oligopeptidase B from Serratia Proteamaculans Revealed a New Type of Inhibitor Binding. *Crystals* **2021**, *11*, 1438. [CrossRef]

17. Fülöp, V.; Szeltner, Z.; Polgár, L. Catalysis of serine oligopeptidases is controlled by a gating filter mechanism. *EMBO Rep.* **2000**, *1*, 277–281. [CrossRef]
18. St-Pierre, J.-F.; Karttunen, M.; Mousseau, N.; Róg, T.; Bunker, A. Use of Umbrella Sampling to Calculate the Entrance/Exit Pathway for Z-Pro-Prolinal Inhibitor in Prolyl Oligopeptidase. *J. Chem. Theory Comput.* **2011**, *7*, 1583–1594. [CrossRef]
19. Kaushik, S.; Sowdhamini, R. Structural Analysis of Prolyl Oligopeptidases Using Molecular Docking and Dynamics: Insights into Conformational Changes and Ligand Binding. *PLoS ONE* **2011**, *6*, e26251. [CrossRef]
20. Szeltner, Z.; Juhász, T.; Szamosi, I.; Rea, D.; Fülöp, V.; Módos, K.; Juliano, L.; Polgár, L. The loops facing the active site of prolyl oligopeptidase are crucial components in substrate gating and specificity. *Biochim. Biophys. Acta (BBA) Proteins Proteom.* **2013**, *1834*, 98–111. [CrossRef]
21. Kaszuba, K.; Róg, T.; Danne, R.; Canning, P.; Fülöp, V.; Juhász, T.; Szeltner, Z.; Pierre, J.-F.S.; García-Horsman, A.; Männistö, P.T.; et al. Molecular dynamics, crystallography and mutagenesis studies on the substrate gating mechanism of prolyl oligopeptidase. *Biochimie* **2012**, *94*, 1398–1411. [CrossRef] [PubMed]
22. Kaushik, S.; Etchebest, C.; Sowdhamini, R. Decoding the structural events in substrate-gating mechanism of eukaryotic prolyl oligopeptidase using normal mode analysis and molecular dynamics simulations. *Proteins Struct. Funct. Bioinform.* **2014**, *82*, 1428–1443. [CrossRef] [PubMed]
23. Swenerton, R.K.; Zhang, S.; Sajid, M.; Medzihradszky, K.F.; Craik, C.S.; Kelly, B.L.; McKerrow, J.H. The Oligopeptidase B of Leishmania Regulates Parasite Enolase and Immune Evasion. *J. Biol. Chem.* **2011**, *286*, 429–440. [CrossRef] [PubMed]
24. Bivona, A.E.; Alberti, A.S.; Matos, M.N.; Cerny, N.; Cardoso, A.C.; Morales, C.; González, G.; Cazorla, S.I.; Malchiodi, E.L. Trypanosoma cruzi 80 kDa prolyl oligopeptidase (Tc80) as a novel immunogen for Chagas disease vaccine. *PLOS Neglected Trop. Dis.* **2018**, *12*, e0006384. [CrossRef] [PubMed]
25. Mikhailova, A.G.; Rakitina, T.V.; Timofeev, V.I.; Karlinsky, D.M.; Korzhenevskiy, D.A.; Agapova, Y.; Vlaskina, A.V.; Ovchinnikova, M.V.; Gorlenko, V.A.; Rumsh, L.D. Activity modulation of the oligopeptidase B from Serratia proteamaculans by site-directed mutagenesis of amino acid residues surrounding catalytic triad histidine. *Biochimie* **2017**, *139*, 125–136. [CrossRef]
26. Petrenko, D.E.; Mikhailova, A.G.; Timofeev, V.I.; Agapova, Y.; Karlinsky, D.M.; Komolov, A.S.; Korzhenevskiy, D.A.; Vlaskina, A.V.; Rumsh, L.D.; Rakitina, T.V. Molecular dynamics complemented by site-directed mutagenesis reveals significant difference between the interdomain salt bridge networks stabilizing oligopeptidases B from bacteria and protozoa in their active conformations. *J. Biomol. Struct. Dyn.* **2019**, *38*, 4868–4882. [CrossRef]
27. Walsh, K.F.; Wilcox, P.E. Serine proteases. *Meth. Enzymol.* **1970**, *19*, 31–41. [CrossRef]
28. Petrenko, D.E.; Nikolaeva, A.Y.; Lazarenko, V.A.; Dorovatovskii, P.V.; Timofeev, V.I.; Vlaskina, A.V.; Korzhenevskiy, D.A.; Mikhailova, A.G.; Rakitina, T.V. Screening of Conditions that Facilitate Crystallization of Oligopeptidase B from Serratia Proteamaculans by Differential Scanning Fluorimetry. *Crystallogr. Rep.* **2020**, *65*, 264–268. [CrossRef]
29. Petrenko, D.E.; Nikolaeva, A.Y.; Lazarenko, V.A.; Dorovatovskiy, P.V.; Timofeev, V.I.; Vlaskina, A.V.; Korzhenevskiy, D.A.; Mikhailova, A.G.; Boyko, K.M.; Rakitina, T.V. Crystallographic Study of Mutants and Complexes of Oligopeptidase B from Serratia proteamaculans. *Crystallogr. Rep.* **2020**, *65*, 909–914. [CrossRef]
30. Long, F.; Vagin, A.A.; Young, P.; Murshudov, G.N. BALBES: A molecular-replacement pipeline. *Acta Crystallogr. Sect. D Biol. Crystallogr.* **2007**, *64*, 125–132. [CrossRef]
31. Murshudov, G.N.; Skubák, P.; Lebedev, A.A.; Pannu, N.S.; Steiner, R.A.; Nicholls, R.A.; Winn, M.D.; Long, F.; Vagin, A.A. REFMAC5 for the refinement of macromolecular crystal structures. *Acta Crystallogr. Sect. D Biol. Crystallogr.* **2011**, *67*, 355–367. [CrossRef]
32. Emsley, P.; Lohkamp, B.; Scott, W.G.; Cowtan, K. Features and development of Coot. *Acta Crystallogr. Sect. D Biol. Crystallogr.* **2010**, *66*, 486–501. [CrossRef] [PubMed]
33. Krissinel, E.; Henrick, K. Inference of Macromolecular Assemblies from Crystalline State. *J. Mol. Biol.* **2007**, *372*, 774–797. [CrossRef]
34. Bond, C.S. TopDraw: A sketchpad for protein structure topology cartoons. *Bioinformatics* **2003**, *19*, 311–312. [CrossRef]
35. Hopkins, J.B.; Gillilan, R.E.; Skou, S. BioXTAS RAW: Improvements to a free open-source program for small-angle X-ray scattering data reduction and analysis. *J. Appl. Crystallogr.* **2017**, *50*, 1545–1553. [CrossRef] [PubMed]
36. Schneidman-Duhovny, D.; Hammel, M.; Tainer, J.A.; Sali, A. Accurate SAXS Profile Computation and its Assessment by Contrast Variation Experiments. *Biophys. J.* **2013**, *105*, 962–974. [CrossRef] [PubMed]
37. Abraham, M.J.; Murtola, T.; Schulz, R.; Páll, S.; Smith, J.C.; Hess, B.; Lindahl, E. GROMACS: High performance molecular simulations through multi-level parallelism from laptops to supercomputers. *SoftwareX* **2015**, *1–2*, 19–25. [CrossRef]
38. Lindorff-Larsen, K.; Piana, S.; Palmo, K.; Maragakis, P.; Klepeis, J.L.; Dror, R.O.; Shaw, D.E. Improved side-chain torsion potentials for the Amber ff99SB protein force field. *Proteins Struct. Funct. Bioinform.* **2010**, *78*, 1950–1958. [CrossRef]
39. Pettersen, E.F.; Goddard, T.D.; Huang, C.C.; Couch, G.S.; Greenblatt, D.M.; Meng, E.C.; Ferrin, T.E. UCSF Chimera-a visualization system for exploratory research and analysis. *J. Comput. Chem.* **2004**, *25*, 1605–1612. [CrossRef]
40. York, D.M.; Darden, T.; Pedersen, L.G. The effect of long-range electrostatic interactions in simulations of macromolecular crystals: A comparison of the Ewald and truncated list methods. *J. Chem. Phys.* **1993**, *99*, 8345–8348. [CrossRef]
41. Kabsch, W.; Sander, C. Dictionary of protein secondary structure: Pattern recognition of hydrogen-bonded and geometrical features. *Biopolymers* **1983**, *22*, 2577–2637. [CrossRef] [PubMed]

42. Joosten, R.; Beek, T.A.H.T.; Krieger, E.; Hekkelman, M.; Hooft, R.; Schneider, R.; Sander, C.; Vriend, G. A series of PDB related databases for everyday needs. *Nucleic Acids Res.* **2010**, *39*, D411–D419. [CrossRef]
43. Amadei, A.; Linssen, A.B.; De Groot, B.L.; Van Aalten, D.M.; Berendsen, H.J. An Efficient Method for Sampling the Essential Subspace of Proteins. *J. Biomol. Struct. Dyn.* **1996**, *13*, 615–625. [CrossRef]
44. Snow, C.; Qi, G.; Hayward, S. Essential dynamics sampling study of adenylate kinase: Comparison to citrate synthase and implication for the hinge and shear mechanisms of domain motions. *Proteins Struct. Funct. Bioinform.* **2007**, *67*, 325–337. [CrossRef]
45. Narzi, D.; Daidone, I.; Amadei, A.; Di Nola, A. Protein Folding Pathways Revealed by Essential Dynamics Sampling. *J. Chem. Theory Comput.* **2008**, *4*, 1940–1948. [CrossRef] [PubMed]
46. Besker, N.; Amadei, A.; D'Abramo, M. Molecular mechanisms of activation in CDK2. *J. Biomol. Struct. Dyn.* **2013**, *32*, 1929–1935. [CrossRef] [PubMed]